Operational Enhancement of Electric Drives by Advanced Cooling Technologies

Benedikt Groschup, Martin Nell and Kay Hameyer, *Senior Member IEEE*
Institute of Electrical Machines (IEM), RWTH Aachen University, 52062 Aachen, Germany

***Abstract*—Heat dissipation determines the power density and Esson's Number of electric motor drives. This paper discusses the thermal influence parameters on Esson's Number. The influencing parameters are studied and discussed in detail. The developed methodology is applied to an induction motor for traction application. Test bench measurements are used to parametrize a thermal reduced order model and study different combinations of rotor and stator cooling technologies, such as natural convection cooling systems of the housing, forced gas and liquid cooling systems of the housing as well as two different types of forced liquid cooling systems of the rotor. The deepened knowledge helps to understand the complex correlations and dependencies in electric machine thermal design processes.**

***Index Terms*—Cooling, Induction Motors, Power Density, Thermal Management, Thermal Modeling, Traction Motors**

I. Introduction

The request for high power density electric motors in traction applications leads to a higher amount of heat that needs to be dissipated from a limited volume. A maximum admissible heat dissipation at critical components must be ensured [1], [2]. For the improvement of heat dissipation in electric machines, several cooling technologies are discussed in literature. A review is given in [3]. In the state of the art rough design process of electric machines like described in [4], Esson's Number C_{mech} is used to obtain a first estimation of the power P_{mech} in dependency of the stator bore diameter D, the active length l_{i}, and the rated speed n_0:

$$P_{\mathrm{mech}} = C_{\mathrm{mech}} D^2 l_{\mathrm{i}} n_0. \tag{1}$$

This paper discusses the thermal influencing parameters on Esson's Number. Therefore, a model is developed. The influence factors are determined and refined, i.e. the heat transfer coefficient, the temperature drop of the cooled component to the temperature of the cooling fluid and the area of the thermal system.

II. Maximum Temperature Thermal Model

A. Cooling Dependent Esson's Number

The losses of the machine P_{loss} can be expressed by using a loss factor ξ depending on the electric machine efficiency and its operational mode:

$$\xi = \begin{cases} \frac{1-\eta}{\eta} & \text{motor mode} \\ 1-\eta & \text{generator mode} \end{cases} \tag{2}$$

$$P_{\mathrm{loss}} = \xi C_{\mathrm{mech}} D^2 l_{\mathrm{i}} n_0. \tag{3}$$

For constant mechanical load in the rotor caused by the centrifugal force, a constant rotor surface velocity v_{ref} can be used [5].

$$v_{\mathrm{ref}} = \pi D n_0 \tag{4}$$

All the losses in the electric machine that are converted into heat $\dot{Q}_{\mathrm{tot}}$, need to be extracted by the heat flow of different cooling methodologies $\dot{Q}_{\mathrm{i}}$ in case of the continuous operational mode.

$$\dot{Q}_{\mathrm{tot}} = P_{\mathrm{loss}} = \sum_{\mathrm{i}} \dot{Q}_{\mathrm{i}}, \tag{5}$$

Three different mechanisms of heat transfer can be considered. As thermal radiation depends on the temperature drop to the power of four and the drop not being sufficiently large in highly utilized electric machines, radiation is neglected in this simplified model. Thermal conduction plays a significant role for the heat flow within the machine, but has a minor impact on the extracted machine losses [6]. In this simplified study, exclusively heat convection is considered,

$$\dot{Q}_{\mathrm{i}} = \alpha_{\mathrm{i}} A_{\mathrm{i}} \Delta T \tag{6}$$

where α is the conduction heat coefficient, A_{i} is the surface area of the thermal system, and ΔT is the temperature drop between the cooled component T_{comp} and the fluid T_{fluid}. Using (3) to (6), Esson's Number C_{mech} can be expressed as:

$$C_{\mathrm{mech}} = \frac{1}{\xi} \frac{\pi}{D l_{\mathrm{i}} v_{\mathrm{ref}}} \sum_{\mathrm{i}} \alpha_{\mathrm{i}} A_{\mathrm{i}} \Delta T. \tag{7}$$

B. Overview of Cooling Capabilities

The capabilities of different cooling concepts i can be combined to increase the maximum possible Esson's Number C_{mech}. For the thermal design of the machine, the three factors α_{i}, A_{i}, and ΔT significantly influence the thermal abilities of the cooling method. Each parameter is described and refined throughout the study, to demonstrate its influence.

978-1-5386-8107-7/19/$31.00 ©2019 IEEE

The area of the thermal system is assumed to be the surface area of the housing circumference. Some correlation factors for the housing diameter $k_{\mathrm{D,ho}}$ and the housing length $k_{\mathrm{L,h}}$ are introduced to refer the formula to the stator bore diameter D and the active length l_{i}, respectively as depicted in Fig. 2:

$$d_{\mathrm{h0}} = k_{\mathrm{D,h0}} \cdot D \tag{8}$$

$$l_{\mathrm{h}} = k_{\mathrm{L,h}} \cdot l_{\mathrm{i}}. \tag{9}$$

The surface area A of this simplified study can be espressed as:

$$A = \pi k_{\mathrm{D,h0}} k_{\mathrm{L,h}} D l. \tag{10}$$

The fluid temperature T_{fluid} is assumed to be the surrounding temperature of 25 °C. The maximum component temperature T_{comp} is limited by the winding temperature [2] with 180 °C. Here, three standard types of convection are studied, i.e. the free convection in gases, the forced convection in gases and the forced convection in liquids. Typical values for the heat transfer coefficient α are shown in Table I [7], [8].

Table I: Assumptions and results of simplified study.

	α in W/m^{2}K			C_{mech} in kW · min/m^3
	[7]	[8]	used	
Free convection in gases	2 - 25	5 - 100	3 - 50	0.12 - 2.07
Forced convection in gases	25 - 250	10 - 350	20 - 300	0.83 - 12.46
Forced convection in liquids	50 - 20000	300 - 3000	200 - 10000	8.31 - 415.3

A range for α is selected as indicated in Table I and used for the calculation of Esson's Number C_{mech}. The first results show a significant deviation of the maximum possible Esson's Number. Whereas with free convection cooling as natural convection of the housing, only small Esson's Numbers can be realized, forced convection of fluids such as water cooling of the housing shows unrealistic high values if compared to literature values smaller than 7 kW · min/m^3 [9] for machines with $P_{\mathrm{mech}} < 1000kW$. The deviations are caused by the significant simplifications and are studied in the following.

III. Advanced Maximum Temperature Thermal Model

In order to obtain realistic results for the maximum Esson's Number, refined expressions for the three factors α_{i}, A_{i}, and ΔT have to be derived.

A. Refined Calculation of α_i

The heat transfer coefficients α_{i} can be calculated with the Nusselt number Nu, the heat conduction coefficient λ and the characteristic length of the thermal system l_{c}.

$$\alpha = \lambda Nu / l_{\mathrm{c}} \tag{11}$$

In highly utilized electric machines, forced flow of fluids is stand of the art cooling technology. In a forced flow system, the Nu number is a function of the fluid dependent Prandl number Pr and the Reynolds number Re that is defined by the flow condition of the problem.

$$Pr = \nu \rho c_{\mathrm{p}} / \lambda \tag{12}$$

An overview of the formula symbols and the resulting Pr number for some fluids that are used in the study is given in Table II, i.e. dry air, water, and mixture of 50 % ethylene glycol and 50 % water (EGW50/50).

Table II: Fluid specifications at 25 °C.

	Symb.	Unit	Dry Air	Water	EGW 50/50
Kinematic viscosity	ν	$\frac{\mu \mathrm{m}^2}{\mathrm{s}}$	15.79	0.8927	2.749
Mass Density	ρ	$\frac{\mathrm{kg}}{\mathrm{m}^3}$	1.169	997.05	1058.3
Specific heat capacity	c_{p}	$\frac{\mathrm{J}}{\mathrm{kg \cdot K}}$	1007	4182	3486.5
Thermal conductivity	λ	$\frac{\mathrm{W}}{\mathrm{m \cdot K}}$	0.02625	0.60652	0.4183
Prandl number	Pr		0.7075	6.1371	24.248

The Re number can be calculated with the velocity of the forced flow ω, the characteristic length of the problem l_{c} and the kinematic viscosity ν.

$$Re = \omega l_{\mathrm{c}} / \nu \tag{13}$$

Circular ducts are a standard problem, commonly found in electric machines, and thus, studied in the following example. The corresponding Nusselt correlation like found in [7] for laminar flow. ($Re < 2300$):

$$Nu_{\mathrm{l}} = (Nu_{\mathrm{l,1}}^3 + 0.7^3 + (Nu_{\mathrm{l,2}} - 0.7)^3 + Nu_{\mathrm{l,3}}^3)^{1/3} \tag{14}$$

$$Nu_{\mathrm{l,1}} = 3.66 \tag{15}$$

$$Nu_{\mathrm{l,2}} = 1.615 \left(Re\, Pr\, \frac{d}{l} \right)^{1/3} \tag{16}$$

$$Nu_{\mathrm{l,3}} = \left(\frac{2}{1 + 22Pr} \right)^{1/6} \left(Re\, Pr\, \frac{d}{l} \right)^{1/2}, \tag{17}$$

where d and l are the diameter of the duct and the length respectively. $Nu_{\mathrm{l,1}}$ is the asymptote for small values of $(Re\, Pr\, d/l)$ and $Nu_{\mathrm{l,1}}$ for large values of $(Re\, Pr\, d/l)$. The therm $Nu_{\mathrm{m,1}}$ is added for short ducts, i.e. high values of d/l.

For turbulent flow with $Re > 10^4$, the following equation is used, [7].

$$Nu_t = \frac{\xi_{\mathrm{t}}/8 RePr}{1 + 12.7\sqrt{\xi_{\mathrm{t}}/8}(Pr^{(2/3)} - 1)} \left(1 + (d_{\mathrm{i}}/l)^{2/3} \right), \tag{18}$$

with:

$$\xi_{\mathrm{t}} = (1.8 \log_{10} Re - 1.5)^{-2}. \tag{19}$$

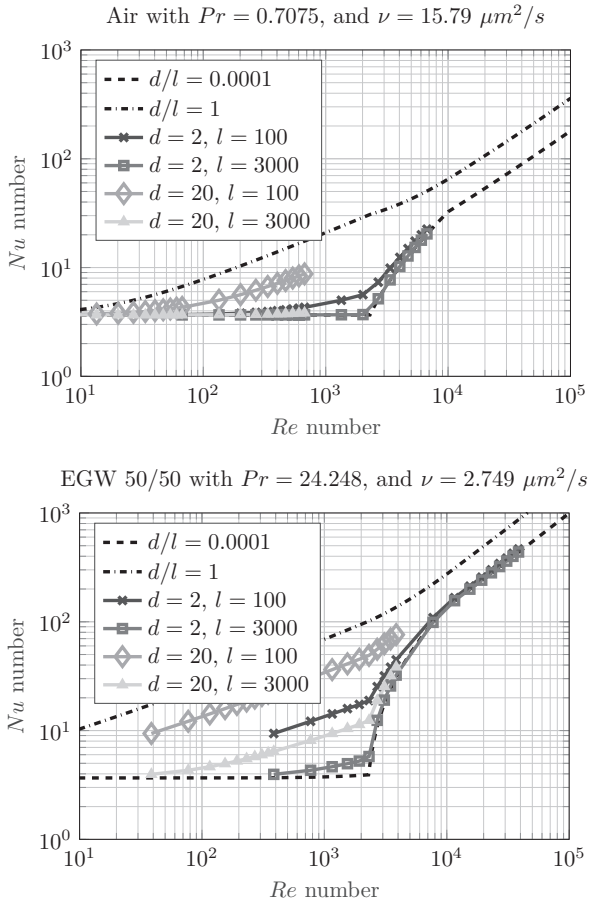

Figure 1: Nu number of EGW 50/50 and dry air for volume flow of 0.1 l/min up to 10 l/min.

For the transition area between laminar and turbulent flow, a transition coefficient γ is defined:

$$\gamma = \frac{Re - 2300}{10^4 - 2300} \text{ and } 0 \leq \gamma \leq 1. \tag{20}$$

The Nu number is calculated based on the coefficient γ, the laminar Nu number for a Re number of $Re = 2300$ and the turbulent result for $Re = 10^4$ [7]:

$$Nu_\mathrm{t} = (1 - \gamma) Nu_{\mathrm{l},2300} + Nu_{\mathrm{t},10^4}. \tag{21}$$

A comparison of the resulting Nu number is given in Fig. 1 for dry air and EGW 50/50. The diameter d is varied in a range of 2 mm that could be used for direct rotor bar cooling up to 20 mm that could be used for shaft cooling or housing cooling. The volume flow is varied between 0.1 L/min and 10 L/min.

All resulting Nu numbers are in between the two dotted lines that represent a short and a high ratio of the d/l. For small Re numbers and small ratios of d/l, the assymptote $Nu_{\mathrm{l},1} = 3.66$ is visible. A turbulent flow is highly requested, as the Nu number significantly increases with a higher Re number, especially above the transition area, i.e. $Re > 10^4$. The hydrodynamical and the thermal development of the flow have a noticeable

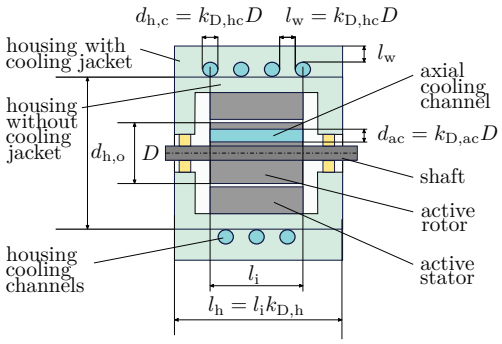

Figure 2: Correlation factors of cooling geometries.

influence on the Nu number which can be seen by comparing the lines with the same diameter d and different lengths l. The comparison of same volume flow rates for different diameters d needs to be considered with caution, as this assumption leads to moderate velocities for ducts with $d = 20$ mm and to unrealistic high velocities for $d = 2$ mm. The flow velocities should be chosen to get Re numbers, resulting in high Nu numbers and heat transition coefficients.

B. Refined Calculation of A_i

For the refinement of the surface area of the thermal system A_i, some more realistic scenarios have to be defined. Therefore, five different cooling methodologies are studied. Correlation factors are used in order to refer the geometry to the same formula symbols like introduced in (7), i.e. D and l_i. An overview of the geometrical dimensions is given in Fig. 2. In the first model, the natural convection of air on the outer circumference of the cylindric housing with the diameter $d_{\mathrm{h},0}$ is used to extract heat. Forced convection of dry air on the cylindric outer circumference of the housing is employed in the second model. For the areas of these two models A_1 and A_2 without a cooling jacket, formula (22) is used.

$$A_{1,2} = \pi k_{\mathrm{D,h0}} k_{\mathrm{L,h}} D l \tag{22}$$

The third model represents a helix shaped cooling of the housing. Therefore, an additional cooling jacket is added to the model and the outer diameter d_h is enlarged as shown in Fig. 2.

$$d_\mathrm{h} = d_{\mathrm{h},0} + 2 d_\mathrm{hc} + 2 l_\mathrm{w} \tag{23}$$

The cooling channels are assumed to be circular ducts with a diameter of $d_{\mathrm{h,c}}$. The axial distance between the cooling channels as well as the distance between a cooling channel and the new outer diameter is assumed to be l_w with,

$$l_\mathrm{w} = d_{\mathrm{h,c}} = k_{\mathrm{D,hc}} D, \tag{24}$$

where $k_{\mathrm{D,hc}}$ is the correlation factor between the helix cooling diameter d_hc and the stator bore diameter D.

The helix is assumed to be placed axially only on the electromagnetic active part of the machine, i.e. the length l_i. The area A_3 of the corresponding problem can be described with:

$$A_3 = \frac{\pi^2}{2}(k_{\mathrm{D,h0}} k_{\mathrm{D,hc}}) D l_\mathrm{i}. \tag{25}$$

The fourth model represents a hollow shaft cooling and the fifth model represents a direct rotor bar cooling. The ducts of the two models are assumed to be placed on the entire active length of the motor l_i with a diameter of d_ac, as shown in Fig. 2. The correlation factor $k_\mathrm{D,ac}$ is used to refer the diameter d_ac to the stator bore diameter D. The area of the thermal system can be expressed with z_ac as the number of axial cooling channels:

$$A_{4,5} = k_\mathrm{D,ac} z_\mathrm{ac} \pi D l_\mathrm{i}. \tag{26}$$

C. Refined Calculation of ΔT

Without using a lumped parameter model, the maximum possible temperature drops of each of the five developed models can be expressed by the difference of the maximum component temperature T_comp of 180 °C for the models with cooled housing ($i = 1, 2, 3$) and for 250 °C for the models with a cooled rotor ($i = 4, 5$). The fluid temperature T_fluid is assumed to be 20 °C for dry air ($i = 1, 2$) and 60 °C for liquid cooling ($i = 3, 4, 5$).

D. Potential of the Thermal Cooling Approaches

For illustration of the potential of each thermal concept, the developed formula is applied to the geometrical cylinder of a sample machine. The used machine is an induction machine with two pole pairs, 36 stator slots and 28 rotor bars. The active length of the machine is $l_\mathrm{i} = 200\,\mathrm{mm}$ and the stator bore diameter is $D = 103\,\mathrm{mm}$. The rated speed of the machine is $n_0 = 3200\,\mathrm{rpm}$ and the rated power is 18.8 kW in continuous operation (S1). An overview of the used correlation factors and the resulting maximum Esson's Number with $\eta = 91\,\%$ is given in Table III.

Table III: Thermal model data and maximum Esson's Number C_mech for each thermal model.

#	Thermal model	$k_\mathrm{D,h0}$	$k_\mathrm{L,h}$	$k_\mathrm{D,hc}$	$k_\mathrm{D,ac}$	z_ac
1	Free; housing	2.1	1.75	–	–	–
2	Forced; housing	2.1	1.75	–	–	–
3	Forced; housing	2.1	1.75	0.1	–	–
4	Forced; shaft	2.1	1.75	–	0.2	1
5	Forced; rotor bar	2.1	1.75	–	0.025	28

#	α in W/(m²K)	A in m²	Index of R	R in K/W	C_mech in kWmin/m³
1	6.6	0.2378	s,Ho-Amb	0.637	0.41
2	71.9	0.2378	s,Ho-Amb	0.0585	4.07
3	3895	0.2236	s,Ho-Amb	0.0011	155.65
4	1242	0.0129	r,cw-fl	0.0622	4.55
5	1893	0.0453	r,cw-fl	0.0117	24.27

The stator cooling concepts 1,2,3 have a higher cooling area than the rotor cooling concepts 4 and 5. The maximum Esson's number for machines with forced flow cooling is still significantly higher than the values found in literature [9].

IV. Thermal Four Node Model

In the previous section, a model assuming a maximum temperature drop ΔT for each component is developed. This assumption is not valid particularly for machines with high performance cooling as a significant share of temperature drop is caused by the preliminary heat-conductive path inside the machine. Therefore, a thermal model of one specific machine design is investigated in the following. A four node model is developed and parametrized with test bench measurements. The model is extended with different cooling methodologies and the influence on continuous operation is studied.

A. Measurements and Parameter Identification

The parameter of the thermal four node model are set by a mix of analytic calculations and parameter identification with the help of measurement data using the test setup like introduced in [10]. The four node model is presented in Fig. 3.

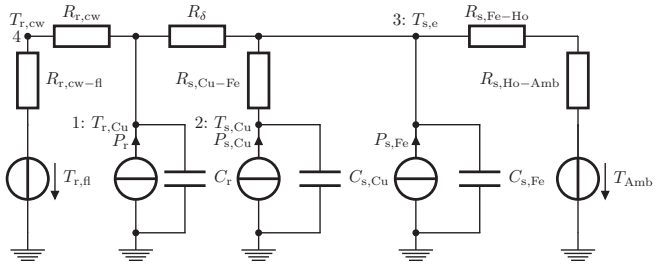

Figure 3: Thermal four node model of an electrical machine.

The measured test bench motor has no rotor cooling and the resistances $R_\mathrm{R,Amb}$ and R_R are assumed to be infinite during parameter identification. $R_\mathrm{R,Amb}$ and R_R are later used for the study. The masses of the rotor components shaft, rotor cage and rotor iron are measured and the heat capacities are estimated based on the known material data, resulting in a total heat capacity of $C_\mathrm{r} = 6.12\,\mathrm{kJ/kg}$. Due to inaccuracies in the material data and some neglected components, such as the lamination glue or the bearings, the heat capacity for the rotor C_r is varied in a range of ±10 % as shown in Table IV.

Table IV: Boundary conditions and results of parameter identification.

Variable	Unit	Lower limit	Upper limit	Calculated data
C_r	kJ/K	5.51	6.73	6.72
$C_\mathrm{s,Fe}$	kJ/K	11.78	13.6	13.22
$\alpha_\mathrm{s,Ho-Amb}$	W/(m² K)	20	300	71.86
$R_\mathrm{s,Cu-Fe}$	K/W	0.03	0.3	0.049

For the airgap resistance R_δ, a Taylor-Couette correlation representing dry air of 100 °C between two flat rotating cylinders is used [9]. The airgap resistance depends on vortices and turbulent flow occurring at higher flow velocities. As the flow velocities are dependent on the machine speed n, the resistance R_δ drops with increasing rotational speed.

The resistance of the stator winding to the stator iron $R_{\mathrm{s,Cu-s,Fe}}$ is determined empirically with a range of 10 W/m²K up to 100 W/m²K. The value of the winding capacity $C_{\mathrm{s,Cu}}$ is set to a fixed value that is calculated from the known copper mass of 4.14 kg and the copper heat capacity of 1.65 kJ/K. The resistances $R_{\mathrm{s,Fe-Ho}}$ are calculated with,

$$R_{\mathrm{s,Fe-Ho}} = \frac{\delta_{\mathrm{int}}}{\lambda_{\mathrm{air,100\,°C}} \cdot A_{\mathrm{int}}}, \tag{27}$$

where $\lambda_{\mathrm{air,100\,°C}}$ is the conductivity of air for 100 °C, A_{int} is the area of the interface and δ_{int} is the thickness of the interface gap. In [6] an average value of 0.037 mm is evaluated for the interface gap width δ_{int}. This value is used resulting in a resistance $R_{\mathrm{s,Fe-Ho}}$ of 0.011 K/m. The temperature $R_{\mathrm{s,Ho-Amb}}$ is determined empirically. The upper and the lower boundary of the resistance are evaluated based on the contact area $A_{1,2}$ of the outer circumference of the motor and the heat transfer coefficient α for forced convection in gases like shown in Table I within a range of 20 W/m²K to 300 W/m²K. Limits of variable parameters in the parameter identification process are shown in Table IV.

Table V: Derivation of temperatures in measurement and simulation.

#	Speed	Torque	Measurement		Simulation	
			Rotor	Winding	Rotor	Winding
1.	1900 min^{-1}	60 N m	136.7 °C	113 °C	134.5 °C	117 °C
2.	3700 min^{-1}	60 N m	171.5 °C	135 °C	180.2 °C	133.5 °C
3.	5700 min^{-1}	37 N m	174.6 °C	135 °C	175 °C	132.9 °C
4.	7500 min^{-1}	26 N m	171.8 °C	135 °C	171.5 °C	135.5 °C

The parameter identification was performed with an evolutionary algorithm and four different temperature measurements of the baseline induction machine in short term operation for 30 minutes. The comparison in Table V shows very good results.

B. Electromagnetic and Thermal Simulation

The efficiency map is calculated in an electromagnetic simulation like introduced in [11] and the calculated losses are introduced into the stator iron $P_{\mathrm{s,Fe}}$, the stator copper $P_{\mathrm{s,Fe}}$ and the rotor iron and copper P_{r}. For the resistances of the rotor channel wall to the rotor fluid $R_{\mathrm{r,cw-fl}}$ and for the stator housing to the ambient $R_{\mathrm{s,Ho-Amb}}$ the resistances, as introduced in Table III, are used. As an example, the efficiency map of the thermal model two that represents the baseline design and the machine with a forced shaft cooling and a forced water cooling in the housing is shown in Fig. 4. The limiting lines for a maximum stator temperature of 180 °C and a maximum rotor temperature of 250 °C are added to the torque speed map.

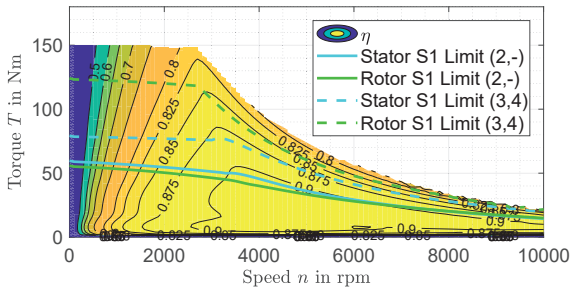

Figure 4: Operatinal limits for continuous operation (S1).

V. Results

The operation point in the torque speed map with maximum power and within both envelopes is added for the comparison in Table VI. For the models one with natural convection on the housing and the advanced rotor cooling models four and five, the stator winding temperature $T_{\mathrm{s,Cu}}$ is limiting the maximum continuous power. For the advanced stator cooling models three and four, the maximum rotor temperature $T_{\mathrm{r,Cu}}$ is limiting. For low performance cooling methodologies like model one, almost all of the potential of the cooling can be used, because the wall temperature of the thermal system $T_{\mathrm{s,ho}} = 176\,°\mathrm{C}$ is close to the maximum winding temperature $T_{\mathrm{s,Cu}} = 180\,°\mathrm{C}$. In this case, a temperature drop of $\Delta T = 156\,°\mathrm{C}$ of the maximum possible drop of $\Delta T = 160\,°\mathrm{C}$ is used. This relative factor is expressed by $\Delta T_{\mathrm{rel}} = 97.5\,\%$ in Table VI.

Table VI: Temperatures modeled by the four node model in °C and C_{mech} in kW · min/m³.

#	limitation		heat transition			η	C_{mech}
	$T_{\mathrm{s,Cu}}$	$T_{\mathrm{r,Cu}}$	$T_{\mathrm{s,Ho}}$	$T_{\mathrm{r,cw}}$	ΔT_{rel}		
1	184.3	198.0	176.0	197.0	97.5 %	0.906	0.4
2	173.54	255.7	116.7	255.7	41.7 %	0.901	2.82
3	144.1	251.5	62.6	251.5	1.4 %	0.883	3.35
4	182.2	127.3	139.8	95.0	28.6 %	0.902	0.86
5	182.4	72.7	107.3	72.7	10.4 %	0.907	1.87

For high potential cooling methodologies, such as model 3, only a small portion of the potential can be exploited, because only a small drop of the temperature occurs between the housing temperature $T_{\mathrm{s,Ho}} = 62.6\,°\mathrm{C}$ and the fluid $T_{\mathrm{fluid}} = 60\,°\mathrm{C}$. A significant share of the temperature drop occurs inside the motor between the critical temperatures $T_{\mathrm{s,Cu}}$, $T_{\mathrm{r,Cu}}$ and the housing temperature $T_{\mathrm{s,Ho}}$. For advanced cooling technologies, the interfaces between the motor components and the heat conduction in the motor play a more significant role. The same study can also be conducted with a combination of rotor and stator cooling technologies as shown in Table VII. The combination of forced rotor bar cooling and forced housing cooling with water shows most significant potential.

Table VII: Results of combination of stator and rotor cooling technologies.

#			4	5
		No Rotor Cooling	Forced, Shaft	Forced, Rotor bar
Stator winding temperature $T_{s,Cu}$ in °C				
	No Stator Cooling	-	182.2	182.4
1	Free, Housing	184.3	180.4	180.6
2	Forced, Housing, Air	173.5	176.0	183.1
3	Forced, Housing, Water	144.0	180.6	182.9
Rotor temperature $T_{r,Cu}$ in °C				
	No Stator Cooling	-	127.4	72.7
1	Free, Housing	198.0	128.2	72.0
2	Forced, Housing, Air	255.7	155.4	75.6
3	Forced, Housing, Water	251.5	185.0	78.6
S1-power P_{S1} in kW				
	No Stator Cooling	-	5.36	11.68
1	Free, Housing	2.69	9.51	14.18
2	Forced, Housing, Air	17.62	22.96	24.85
3	Forced, Housing, Water	20.96	27.41	28.01
Esson's Number C_{mech} in kW $\cdot$ min/m^3				
	No Stator Cooling	-	0.85	1.87
1	Free, Housing	0.4	1.52	2.27
2	Forced, Housing, Air	2.82	3.67	3.98
3	Forced, Housing, Water	3.36	4.39	4.49

VI. Conclusions and Further Work

The influence of thermal cooling on electric machines operational limits has been studied. The thermal influencing factors α, ΔT and A have been examined for different cooling methods, fluids and flow conditions.The models were parametrized by measurement data and extended by alternative cooling methodologies. The forced flow of liquids has shown a high potential for low power density motors. In an electric machine design with advanced cooling technology, the conduction within the machine gains importance. The quality of stator and rotor cooling technologies influence each other. The developed methodology can be used to improve the design of a specific application by selecting the proper cooling methodology. In future work, the interfaces and heat paths within the motor have to be studied in more detail.

References

[1] M. Jaeger, A. Ruf, K. Hameyer, and T. G.-v. Tongeln, "Thermal analysis of an electrical traction motor with an air cooled rotor," in *2018 IEEE Transportation and Electrification Conference and Expo (ITEC)*. Piscataway, NJ: IEEE, 2018, pp. 467–470.

[2] A. Ruf, J. Paustenbach, D. Franck, and K. Hameyer, "A methodology to identify electrical ageing of winding insulation systems," in *2017 IEEE International Electric Machines and Drives Conference (IEMDC)*. IEEE, 2017, pp. 1–7.

[3] M. Popescu, D. A. Staton, A. Boglietti, A. Cavagnino, D. Hawkins, and J. Goss, "Modern heat extraction systems for power traction machines—a review," *IEEE Transactions on Industry Applications*, vol. 52, no. 3, pp. 2167–2175, 2016.

[4] D. Gerling, *Electrical Machines: Mathematical Fundamentals of Machine Topologies*, ser. Mathematical Engineering. Berlin, Heidelberg: Springer Berlin Heidelberg, 2015, vol. 4.

[5] B. Groschup and F. Leonardi, "Combined electromagnetic and static structural simulation to reduce the weight of a permanent magnet machine rotor for hev application," in *2017 IEEE International Electric Machines and Drives Conference (IEMDC)*. IEEE, 2017, pp. 1–6.

[6] D. Staton, A. Boglietti, and A. Cavagnino, "Solving the more difficult aspects of electric motor thermal analysis in small and medium size industrial induction motors," *IEEE Transaction on energy conversion*, vol. 20, no. 3, pp. 620–628, September 2005.

[7] P. Stephan, S. Kabelac, M. Kind, H. Martin, D. Mewes, and K. Schaber, *VDI heat atlas*, 2nd ed., ser. VDI-Book. Berlin: Springer-Verlag, 2010.

[8] S. M. S. Murshed, Ed., *Electronics Cooling*. InTechOpen, 2016.

[9] J. Pyrhönen, T. Jokinen, and V. Hrabovcová, *Design of rotating electrical machines*. John Wiley & Sons, Ltd, 2008.

[10] M. Nell, G. von Pfingsten, and K. Hameyer, "Rapid parameter identification and control of an induction machine," *The international journal for computation and mathematics in electrical and electronic engineering (COMPEL)*, vol. 37, no. 5, pp. 1678–1688, 2018.

[11] M. Nell, J. Lenz, and K. Hameyer, "Efficient numerical optimization of induction machines by scaled fe simulations," in *2018 XIII International Conference on Electrical Machines (ICEM)*, Sept 2018, pp. 198–204.

VII. Biographies

Benedikt Groschup was born in Würzburg, Germany, on March 13th, 1990. He recieved his Master's degree in Automotive Engineering and Transport in September 2015 at RWTH Aachen University in colaboration with Ford Motor Company in Detroit, Michigan, USA.
He started working as a research associate of RWTH Aachen University in February 2016. His research interests include induction and permanent magnet motor modeling, iron loss calculation in macroscopic scale, vehicle modeling and thermal modeling.

Martin Nell was born in Koblenz in Germany, on July 11, 1990. He received his Master's degree in April 2017 in Electrical Engineering from RWTH Aachen University, Germany.
He has been working as a research associate at the Institute of Electrical Machines since May 2017. His research interests include induction machine modeling, optimization of induction machines, iron loss calculation in macroscopic scale and vehicle modeling

Dr. Kay Hameyer received his M.Sc. degree in electrical engineering from the University of Hannover and his Ph.D. degree from the Berlin University of Technology, Germany. After his university studies he worked with the Robert Bosch GmbH in Stuttgart, Germany as a Design Engineer for permanent magnet servo motors and vehicle board net components. From 1996 to 2004 Dr. Hameyer was a full Professor for Numerical Field Computations and Electrical Machines with the KU Leuven in Belgium. Since 2004, he is full Professor and the director of the Institute of Electrical Machines (IEM) at RWTH Aachen University in Germany. 2006 he was vice dean of the faculty and from 2007 to 2009 he was the dean of the faculty of Electrical Engineering and Information Technology of RWTH Aachen University. His research interests are numerical field computation and optimization, the design and controls of electrical machines, in particular permanent magnet excited machines and induction machines. Since several years Dr. Hameyer's work is concerned with magnetically excited audible noise in electrical machines, the life time estimation of insulating systems and the characterization of ferro-magnetic materials. Dr. Hameyer is author of more than 250 journal publications, more than 700 international conference publications and author of 4 books. Dr. Hameyer is a member of VDE, IEEE senior member, fellow of the IET.